Kong, Gyuyeol; Jung, Minchae; Koivunen, Visa

Waveform Classification in Radar-Communications Coexistence Scenarios

Published in:
2020 IEEE Global Communications Conference, GLOBECOM 2020 - Proceedings

DOI:
10.1109/GLOBECOM42002.2020.9322442

Published: 01/01/2020

Document Version
Peer reviewed version

Waveform Classification in Radar-Communications Coexistence Scenarios

Gyuyeol Kong*, Minchae Jung†, and Visa Koivunen*
*Department of Signal Processing and Acoustics, Aalto University, Espoo, Finland
Email: {gyuyeol.kong and visa.koivunen}@aalto.fi
†Wireless@VT, Department of Electrical and Computer Engineering, Virginia Tech, VA, USA
Email: hosaly@vt.edu

***Abstract*—In this paper the problem of recognizing waveform and modulation is addressed in radar-communications coexistence and shared spectrum scenarios. We propose a deep learning method for waveform classification. A hierarchical recognition approach is employed. The received complex-valued signal is first classified to single carrier radar, communication or multicarrier waveforms. Fourier synchrosqueezing transformation (FSST) time-frequency representation is computed and used as an input to a convolutional neural network (CNN). For multicarrier signals, key waveform parameters including the cyclic prefix (CP) duration, number of subcarriers and subcarrier spacing are estimated. The modulation type used for subcarriers is recognized. Independent component analysis (ICA) is used to enforce independence of I- and Q-components, and consequently significantly improving the classification performance. Simulation results demonstrate the high classification performance of the proposed method even for orthogonal frequency division multiplexing (OFDM) signals with high-order quadrature amplitude modulation (QAM).**

***Index Terms*—Signal intelligence, waveform recognition, Fourier synchrosqueezing transform, independent component analysis, convolutional neural network**

I. Introduction

Wireless signal recognition plays an important role in cognitive radio and radar systems. It enables spectrum monitoring and management for co-existence of radar and communications, RF sensing and communication in vehicular applications [1], [2]. In shared spectrum environments, many different waveforms are used in the same spectrum making the classification task more challenging. A variety of machine learning methods in the radar waveform recognition [3]–[5] and in the modulation classification for wireless communications [6], [7] have been introduced. However, waveform recognition in shared spectrum and radar-communication coexistence scenarios has not been studied. The presence of both radar and communication signals in the same observed data makes considerably more difficult to classify the waveforms reliably. Also, the radar waveform recognition methods based on the Choi-Williams distribution (CWD) [3]–[5] have been considered only in additive white Gaussian noise (AWGN) channel. However, the realistic wireless channels are subject to multipath fading and the CWD neglects the important phase information due to the second order statistic. In addition, only single carrier waveform is used in [6]. Recognition of orthogonal frequency division multiplexing (OFDM) waveforms is considered assuming AWGN channel in [7]. Obviously, classification in multipath fading is significantly more complicated.

We propose a hierarchical machine learning approach for recognizing waveforms and modulation classes in radar-communications coexistence and shared spectrum scenarios over AWGN and multipath fading channels. The proposed method classifies first the signals into three subclasses: single and multicarrier communication signals and radar signals. Then, separate classifiers are applied to each subclass. The method employs two deep convolutional neural network (CNN) structures. The first CNN recognizes the subclass based on complex-valued time-frequency representation computed using Fourier synchrosqueezing transform (FSST). The FSST has powerful properties in revealing behavior, rate of, strength and number of oscillatory components in signal [10]. The actual modulation class and some important waveform parameters are then determined in the second stage by a subclass classifier. In this paper, we describe the subclassifier for multicarrier signals in more detail. The subclassifier for radar waveforms in our system has been described in [8], [9].

In addition to recognizing modulation type, the key transmission parameters of signals are estimated from the received signal. Here, we focus on OFDM parameters. The cyclic prefix (CP) duration is estimated by using inherent correlation feature of the received signal caused by the CP [7]. Then, the number of subcarriers and carrier spacing are estimated based on the eigenvalues of autocovariance matrix of the received signal by applying the minimum description length (MDL) [11] and multiple signal classification (MUSIC) [12] methods, respectively. After isolating the subcarrier signal using the fast Fourier transform (FFT) with the estimated parameters, the second CNN classifies quadrature amplitude modulation (QAM) of the multicarrier waveforms. Blind source separation (BSS) using an independent component analysis (ICA) [13] is applied to complex-valued observations as a preprocessing step. It enforces the I- and Q-components to be as independent as possible. Consequently, it makes the recognition easier since the impact of rotation of constellations is reduced from the classification task. The BSS extracts the I- and Q-components of original modulated signal from the received signal of each subcarrier experiencing flat fading. By using the BSS, the key properties of high-order QAM are better revealed and the classification task can be performed reliably.

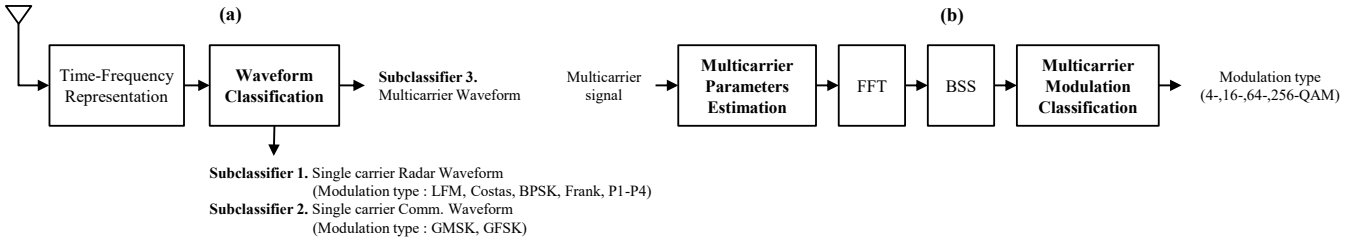

Fig. 1. Block diagram of the proposed method. (a) Hierarchical structure for waveform classification (b) Subclassifier for multicarrier signals

II. System and Waveforms

In this section, we present the system model and waveforms considered in this paper. For waveform classification, the hierarchical classifier first selects one of three subclassifiers for radar, singe carrier and multicarrier communication waveforms. We assume that the observed signals have been transmitted over multipath fading channels. Let $s(t)$ denote the complex transmitted signal at time t and $n(t)$ denote the AWGN with the variance σ_n^2. Then, the continuous-time complex-valued received signal $y(t)$ can be expressed as

$$y(t) = \sum_{n=0}^{\ell-1} \alpha_n(t)\, s(t-\tau_n) + n(t), \tag{1}$$

where ℓ represents the number of path delays, α_n is the complex channel coefficient at the n-th path delay, and τ_n is the n-th path delay. For the Doppler shift, we considered the maximum Doppler frequency f_D.

We recognize three broad waveform types in this paper that is radar, single carrier communication and multicarrier OFDM waveforms. In case of single carrier waveforms, we distinguish between radar and communication signals and select the subclassifier accordingly. For the multicarrier signals, the modulation method used for subcarriers is recognized and key waveform parameters are determined. Among the parameters are intercarrier spacing, duration of a guard interval or cyclic prefix and well as number of modulated subcarriers. For the radar waveforms, we consider eight modulations, the linear frequency modulation (LFM), Costas, binary phase shift keying (BPSK) and five polyphase codes such as Frank, P1, P2, P3 and P4 codes with the parameters used in [8], [9]. For the communication waveforms, we consider single carrier waveform with Gaussian minimum shift keying (GMSK) and frequency modulated shift keying (FMSK) and OFDM waveform with Q-ary QAM (Q-QAM) for Q = 4, 16, 64 and 256. Thus, a total of 14 classes are considered in recognizing waveform and modulation.

III. Proposed Waveform and Modulation Classification Method

In this section, we present the waveform and modulation classification approach for radar-communications coexistence systems and shared spectrum scenarios. The proposed method performs a hierarchical classification for waveform and modulation classification as shown in Fig. 1. First, the method selects one of the three subclassifiers based on a time-frequency representation of the intercepted signal. In the subclassifiers for single carrier radar and communication signals, the modulation type is determined among the categories of the classified subclassifier. The subclassifier for multicarrier signals performs both modulation recognition for subcarrier signals and multicarrier transmission parameter estimation. The parameters of interest include the CP duration, number of subcarriers and subcarrier spacing are estimated. After the FFT with the estimated parameters, the multicarrier modulation classifier classifies the modulation type of the multicarrier waveform using the BSS as a preprocessing step and CNN.

A. Higher Level Classifier

This section describes the higher level classification as shown in Fig. 1(a). This stage classifies the single carrier radar and communication waveforms and multicarrier waveform based on their time-frequency properties. In the waveform classification, two steps are processed, the time-frequency representation and the classification based on CNN.

1) Time-frequency representation: There are three phases to make input image data of the CNN. First, the continuous-time received signal $y(t)$ is sampled to the discrete-time received signal $\mathbf{y} = [y[0], \ldots y[M-1]]^T$ of size $M \times 1$ with a sampling frequency f_s, where M is the number of time-domain samples. Second, the $\mathbf{y}$ is transformed into the time-frequency representation using the FSST described by R spectrum values in frequency bins for M time-domain samples. The FSST is a kind of time-frequency transform which is an effective approach to provide a concentrated representation of multicomponent signals in time-frequency plane [10]. Therefore, we create the complex-valued bivariate image of size of 128 (R) $\times$ 2048 (M) from the FSST when we considered R = 128 and M = 2048. Lastly, the bivariate image with size of 128$\times$2048 is reshaped into $I \times I$ pixels for the input of CNN in order to reduce the computation load. For the image resizing, we set I = 128 and the nearest neighbor interpolation (NNI) technique [14] is used. As a result, the size of image for the input of the CNN is 128$\times$128$\times$2, because the NNI process is separately operated for the real and imaginary parts of image.

The proposed method determines the waveform type by selecting one of three subclasses for radar and single and multicarrier communication waveforms based on the probabilities for 11 categories. The 11 categories include the eight

radar signals, two single carrier communication signals and multicarrier signal by combining four QAM into one category. The subclass corresponding to the peak value among probabilities for 11 categories is selected, where the probabilities are calculated from Softmax of the CNN classifier. In cases of the radar and single carrier communication subclasses, the modulation class with the peak value is determined in the subclassifier. The process of subclassifier for radar waveforms has been presented in [8], [9]. For multicarrier subclass, the subclassifier estimates the multicarrier parameters and classifies the modulation class of each subcarrier using the BSS as a preprocessing step and CNN.

2) Deep CNN classifier: The deep CNN presented in [9] is applied for waveform classification. In the input layer, the resized image of size 128×128×2 generated in the image preprocessing step is used as an input to the CNN. For the convolutional layer, the numbers of convolution filters for the first, second and third layers are set to 8, 16 and 32 with the filter size 3×3, respectively. For the pooling layer, we use the max and average pooling with 2×2 filter size, stride size 2 and no zero-padding. The exponential linear unit (ELU) is used as the activation function layers except the output layer where Softmax was employed. In the fully connected (FC) layers, the number of neurons for the second FC layer is 128. In the output layer, Softmax consisting of 11 nodes for 11 categories calculates probabilities to each class.

B. Multicarrier Waveform Parameter Estimation

This section describes the multicarrier parameters estimation performed in subclassifier 3 of Fig. 1. Estimating the number of subcarriers, subcarrier spacing and CP duration are needed to provide full characterization of the multicarrier waveform, perform the FFT at the receiver and recognize modulation class used for individual subcarriers. We presents methods of estimating these parameters by applying signal processing techniques.

1) CP duration estimation: The correlation process was performed on the discrete-time received OFDM signal for estimating CP duration T_{cp}. In the OFDM waveform, the duplicated signal, referred to as CP, generated by the last T_{cp} portion of the data symbol period T_b is added to the front of the data symbol. Then, the total duration of the transmitted OFDM symbol is an addition of data symbol duration with the CP duration, $T_s = T_{cp} + T_b$. By exploiting the inherent correlation feature caused by the CP in an OFDM signal, autocorrelation based method for estimating T_{cp} is employed. The autocorrection process is given by

$$r[\tau] = \sum\nolimits_{i=-\infty}^{\infty} y[i+m-\tau]y^*[i], \quad 0 < \tau < m, \quad (2)$$

where $r[\tau]$ is the autocorrelation value with the delay index τ, m is the number of samples for a single OFDM symbol, $y[i]$ is the discrete-time received signal at the sample index i during N OFDM symbol observations, $0 \le i \le N \cdot m - 1$, and $y^*[k]$ means the complex conjugate of $y[k]$. From the autocorrelation process, a peak can be observed at delay τ. Then, the duration of τ is estimated to be the estimated CP duration $\hat{T}_{cp}$.

2) Estimating the number of subcarriers: The MDL model order estimation algorithm is applied to detect the number of signal sources for estimating the number of subcarriers P corresponding to the FFT size N_{FFT}. Once the CP duration $\hat{T}_{cp}$ is determined, it is removed from the OFDM symbol, and the sample autocovariance matrix is calculated based on the part of data symbols for the MDL algorithm. The MDL algorithm [11] is used to determines the number of sinusoidal signals in the received waveform since OFDM signal is constructed as a sum of modulated sinusoids. After eliminating the CP, the discrete-time received signal $\mathbf{y}_n$ of size $M \times 1$ is obtained with the sampling frequency f_s at the n-th OFDM symbol. Then, the $M \times M$ sample autocovariance matrix is obtained as $\hat{\mathbf{R}}_y = 1/N \sum_{n=1}^{N} \mathbf{y}_n \mathbf{y}_n^H$, where N is the total number of OFDM symbol. The eigenvalues arranged in decreasing order λ_i, $i = 1, \cdots, M$, are obtained from the eigen decomposition of $\hat{\mathbf{R}}_y$. Then, the MDL criterion for the number of subcarriers P is [11]:

$$\hat{P} = \arg \min_{k=0,1,\ldots,M-1} \mathrm{MDL}\,(k)\,, \quad (3)$$

where

$$\begin{aligned} \mathrm{MDL}\,(k) = N\,(M-k) \log \frac{1/(M-k)\sum_{i=k+1}^{M} \lambda_i}{\left(\prod_{i=k+1}^{M} \lambda_i\right)^{1/(M-k)}} \\ + \frac{1}{2} k\,(2M-k) \log N. \end{aligned} \quad (4)$$

3) Subcarrier spacing estimation: The MUSIC high resolution frequency estimation algorithm [12] is employed to detect subcarrier spacing Δf based on the $\hat{\mathbf{R}}_y$ and $\hat{P}$. Let $\mathbf{v}_i$ be eigenvector of $\hat{\mathbf{R}}_y$ corresponding to λ_i, $i = 1, \cdots, M$, arranged in decreasing order. Then, the MUSIC algorithm for estimating Δf is expressed as

$$\hat{P}_{MUSIC}\left(e^{j\omega}\right) = \frac{1}{\sum_{i=p+1}^{M} \left|\mathbf{e}^H \mathbf{v}_i\right|^2}, \quad (5)$$

where p is the number of complex exponentials in the OFDM waveform and $\mathbf{e}$ is the vector of complex exponentials $e^{jk\omega}$, $k = 1, \cdots, p$, $\mathbf{e} = \left[1, e^{j\omega}, \ldots, e^{jp\omega}\right]^T$. We regarded $\hat{P}$ from the MDL algorithm as p. The frequencies of the complex exponentials $\hat{\omega}_i$, $i = 1, \cdots, \hat{P}$, are taken as the locations of the $\hat{P}$ largest peaks in $\hat{P}_{MUSIC}\left(e^{j\omega}\right)$. By measuring the spacing between $\hat{\omega}_i$, the estimated subcarrier spacing between subcarriers $\Delta \hat{f}_i$ are obtained for $i = 1, \cdots, \hat{P} - 1$.

C. Multicarrier Signal Classification

This section describes the multicarrier signal classification stage. After the FFT operation with estimated T_{cp}, P and Δf, this stage classifies the modulation of OFDM waveform. This stage uses the BSS method, in particular ICA as a preprocessing step for the CNN based classification as explained below.

1) BSS based on ICA: The BSS technique is used to make the real and imaginary components of the received signal as independent as possible. This is a common property for most digital modulation methods used in practice. No prior knowledge of the actual modulation scheme or channel state

TABLE I
STRUCTURE OF THE EMPLOYED CNN WITH THE BSS INPUT FOR THE MODULATION CLASSIFICATION PROBLEM.

Layer	Dimension	Parameters	Activation
Input	(2,2048)	-	-
Convolution 1D	(2,2048,16)	144	-
Batch Normalization	(2,2048,16)	16	ELU
Max Pooling 1D	(2,1024,16)	-	-
Convolution 1D	(2,1024,24)	3,096	-
Batch Normalization	(2,1024,24)	24	ELU
Max Pooling 1D	(2,512,24)	-	-
Convolution 1D	(2,512,32)	4,640	-
Batch Normalization	(2,512,32)	32	ELU
Max Pooling 1D	(2,256,32)	-	-
Convolution 1D	(2,256,48)	6,176	-
Batch Normalization	(2,256,48)	48	ELU
Max Pooling 1D	(2,128,48)	-	-
Convolution 1D	(2,128,64)	24,640	-
Batch Normalization	(2,128,64)	64	ELU
Max Pooling 1D	(2,64,64)	-	-
Convolution 1D	(2,64,96)	49,248	-
Batch Normalization	(2,64,96)	96	ELU
Avg Pooling 1D	(2,1,96)	-	-
Flatten	-	-	-
FC (Dense)	(192)	772	ELU
Dense	(5)	-	Softmax

information is required. In the OFDM transmission, each subcarrier experiences flat fading even though the overall broadband signal suffers from frequency-selective fading. Let $\mathbf{s}(k)$ denote the transmitted signal vector of size $1\times L$ at the k-th subcarrier with the L OFDM symbols, and $h(k)$ denote the complex single tap channel coefficient at the k-th subcarrier. Then, the received signal vector of size $1 \times L$ at the k-th subcarrier $\mathbf{y}(k)$ is given by

$$\mathbf{y}(k) = h(k) \cdot \mathbf{s}(k) + \mathbf{n}(k), \quad k = 1, \ldots, N_{FFT}, \qquad (6)$$

where $\mathbf{n}^{(\mathbf{s})}$ is the AWGN vector of size $1 \times L$ at the s-th subcarrier. We assume quasistationarity, that is the channel coefficient $h(k)$ remains constant during the transmission of L OFDM symbols for each subcarrier. In the OFDM waveform, the received signal $\mathbf{y}(k)$ can be expressed as the mixture of $\mathbf{s}(k)$ in relation to $h(k)$. Let $\mathbf{S}(k)$ be $2\times L$ matrix with real and imaginary components of source signal $\mathbf{s}(k)$ in the two row vectors. Then, the ICA linear mixed model in each subcarrier can be expressed as

$$\mathbf{X}(k) = \mathbf{A}(k)\mathbf{S}(k) + \mathbf{N}(k), \quad k = 1, \ldots, N_{FFT}, \qquad (7)$$

where $\mathbf{X}(k)$ is an observed mixture of I- and Q-signals of dimension $2 \times L$, $\mathbf{A}(k)$ is a 2×2 mixing matrix, and $\mathbf{N}(k)$ is the AWGN vector. After centering and whitening of $\mathbf{X}(k)$, the BSS technique finds the orthogonal 2×2 demixing matrix $\mathbf{W}(k)$ to estimate sources as $\hat{\mathbf{S}}(k) = \mathbf{W}(k)\mathbf{X}(k)$. For the BSS technique, a power iteration based fast independent component analysis (PowerICA) [15] is employed, which is more stable than the well-known FastICA separation [16]. The estimated sources $\hat{\mathbf{S}}(k)$ from the PowerICA are used as the input of the CNN classifier to perform the classification task. In this paper, we considered $L = 2048$. As a result, the size of data for the input of the CNN is 2×2048.

2) Multicarrier Modulation classification based on CNN: The modulation classification uses a deep CNN with six covolutional layer and a FC layer described in Table I. Unlike the CNN for the waveform classification based on the time-frequency representation, the CNN for the modulation classification considers the time-domain signal as an input to the classifier. Because the Q-QAM signals are defined as the random shift of the magnitude and phase components according to message, they do not include specific characteristics in the frequency domain. The CNN for the modulation classification consists of an input layer, six convolutional layers, six batch normalization layers, six pooling layers, a FC layer, and an output layer. In the input layer, the estimated sources of size 2×2048 from the BSS technique is used as the input of the CNN. For the convolutional and pooling layers, the convolutional and pooling filter sizes are changed from the 2D array to the 1D array. In the convolutional layer, the convolutional filter of size 1×8 is used, and in the pooling layer the pooling with the filter sizes 1×2 and 1×64 are used for the max and average pooling, respectively. In the output layer, Softmax consisting of five nodes computes probabilities for each class. Based on the probabilities obtained in Softmax, the CNN classifies the signal to belong to one of the Q-QAM classes, Q = 4, 16, 64, 256.

TABLE II
CONFUSION MATRIX OF WAVEFORM CLASSIFICATION AT SNR OF 0 dB. THE OVERALL CLASSIFICATION RATE IS 98.9%.

	LFM	Costas	BPSK	Frank	P1	P2	P3	P4	GFSK	GMSK	OFDM
LFM	100	0	0	0	0	0	0	0	0	0	0
Costas	0	100	0	0	0	0	0	0	0	0	0
BPSK	0	0	100	0	0	0	0	0	0	0	0
Frank	0	0	0	100	0	0	0	0	0	0	0
P1	0	0	0	0	97.8	0	0	2.2	0	0	0
P2	0	0	0	0	0	100	0	0	0	0	0
P3	0	0	0	0	0	0	100	0	0	0	0
P4	0	0	0	0	1.9	0	0	98.1	0	0	0
GFSK	0	0	0	0	0	0	0	0	100	0	0
GMSK	0	0	0	0	0	0	0	0	0	96.8	3.2
OFDM	0	0	0	0	0	0	0	0	0	5.0	95.0

IV. SIMULATION RESULTS

In this section, we evaluated the performances of the waveform and modulation classification and multicarrier parameters estimation in AWGN and multipath fading channels. First, the waveform classification performance of the hierarchical classifier classifying three subclassifiers for the radar and single and multicarrier communication waveforms is evaluated. Then, the estimation performances are evaluated for T_{cp}, P and Δf for multicarrier subclass. Lastly, the modulation classification performance of the subclassifier for the multicarrier waveform is evaluated. We used the root mean squared error (RMSE) for the estimation performance and probability of correct classification P_{cc} for the classification performance.

We used a Kaiser window of length 128 with shape parameter β = 10 for the FSST and $f_s = 30.74MHz$ for the sampling frequency. For the multipath fading channels, extended vehicular A model (EVA) with $f_D = 70Hz$ is used [17] in the communication waveforms, and Rician channel model in [9] is used in the radar waveforms. For the training and test processes of the CNN, we generated 10,000 signals

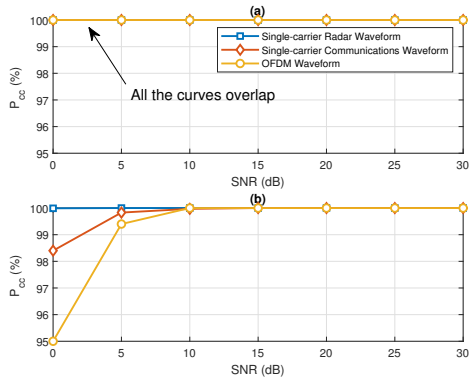

Fig. 2. Classification performances of the waveform classification as a function of SNR. (a) AWGN and (b) multipath fading channels.

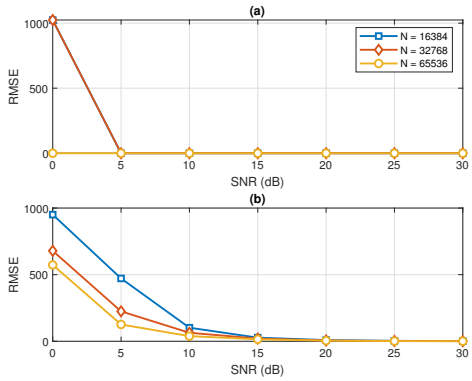

Fig. 4. Estimation performances of $\hat{P}$ with N_{FFT} = 1024 as a function of SNR. (a) AWGN and (b) EVA channels.

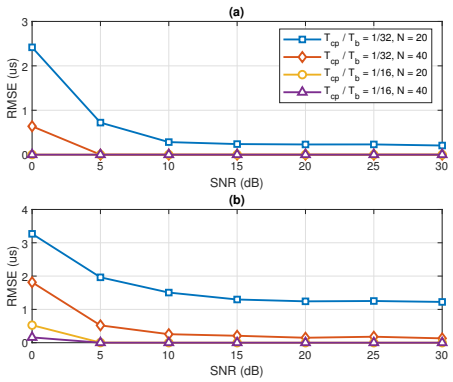

Fig. 3. Estimation performances of $\hat{T}_{cp}$ with N_{FFT} = 1024 as a function of SNR. (a) AWGN and (b) EVA channels.

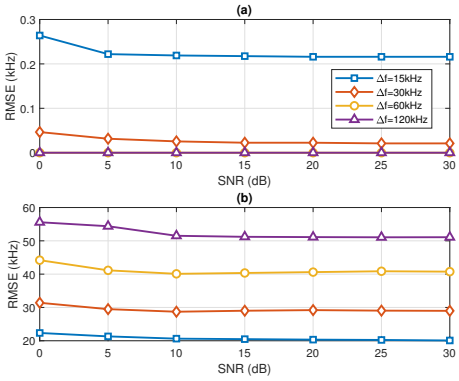

Fig. 5. Estimation performances of $\Delta\hat{f}_i$ with N_{FFT} = 1024 as a function of SNR. (a) AWGN and (b) EVA channels.

for each of the eight radar waveforms, two single carrier communication waveforms and OFDM waveform in waveform classification and for each of the four QAM modulations in OFDM modulation classification with signal-to-noise ratio (SNR) ranging from 0 dB to 30 dB at a step size of 5 dB. The SNR is defined as $\mathrm{SNR\,(dB)} = 10\log_{10}\left(E_s/\sigma_n^2\right)$, where E_s is the the signal power. Therefore, the total numbers of signal are 110,000 and 40,000 per SNR for waveform and OFDM modulation classification, respectively. In each signal, 80% and 20% of the signals were used as the training and validation sets, respectively. The CNN was trained over 50 epochs using Adam optimizer with the initial learning rate 10^{-3} [18]. In the training process, we used the mini-batch gradient descent algorithm with the batch size of 64 that splits the training dataset into small batches to estimate the error gradient before the model weights are updated.

Table II shows the confusion matrix of the waveform classification at SNR of 0 dB in multipath fading channel. The confusion matrix indicates that the radar and communication waveforms are clearly classified, but the discrimination between GMSK and OFDM waveforms is somewhat difficult. In the radar waveforms, the P1 and P4 codes that are usually difficult to distinguish [8], [9] have the relatively lower classification performances compared to the other radar waveforms.

Figure 2 shows the P_{cc} of the waveform classification as a function of SNR in AWGN and multipath fading channels. In AWGN channel, 11 waveforms specified in Table II are perfectly classified. However, the communication waveforms experiencing EVA channel are somewhat difficult to distinguish compared to the radar waveforms experiencing Rician channel at low SNR regime. At SNR above 10 dB, 11 waveforms are also perfectly classified in EVA channel.

Figure 3 shows the RMSE of $\hat{T}_{cp}$ with N_{FFT} = 1024 as a function of SNR. The RMSE of $\hat{T}_{cp}$ becomes gradually lower as N increases. Also, the RMSE of the longer CP duration with $T_{cp}/T_b = 1/16$ is lower than that of the shorter CP duration with $T_{cp}/T_b = 1/32$. Although the RMSE of EVA channel are more degraded than that of AWGN channel, the RMSE of $\hat{T}_{cp}$ is close to zero even in EVA channel at SNR above 5 dB when N is considered as 40.

Figure 4 shows the RMSE of $\hat{P}$ with N_{FFT} = 1024 as a function of SNR. The RMSE of $\hat{P}$ is getting improved as the number of observation N increases in AWGN and EVA channels. When N is considered as 65,536, the RMSE of $\hat{P}$ is 0 even at SNR of 0 dB in AWGN channel, while it approaches zero at SNR regime above 10 dB in EVA channel.

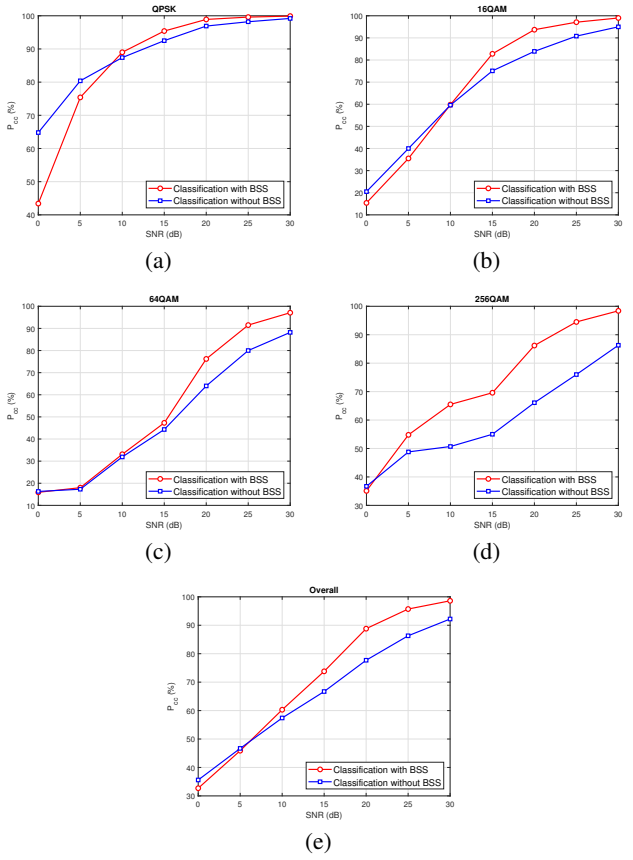

Fig. 6. Modulation classification performances for the multicarrier waveform in EVA channel as a function of SNR. (a) 4-QAM, (b) 16-QAM, (c) 64-QAM, (d) 256-QAM and (e) Overall

Figure 5 shows the RMSE of $\Delta\hat{f}_i$ with N_{FFT} = 1024 as a function of SNR. The RMSE of $\Delta\hat{f}_i$ gradually increases as Δf increases in EVA channel due to the multipath fading effect, while the RMSE of $\Delta\hat{f}_i$ becomes gradually lower as Δf increases in AWGN channel. Although the RMSE performance degradation occurs in EVA channel, Δf can be perfectly estimated by the majority vote of $\Delta\hat{f}_i$ for all subcarriers in AWGN and EVA channels.

Figure 6 shows the modulation classification performances for the multicarrier waveform in EVA channel as a function of SNR. The overall P_{cc} of classification with BSS has the better performance than that of classification without BSS at SNR above 10 dB. At SNR below 10 dB, the classification with BSS shows the worse performance than the classification without BSS because enforcing independence of I- and Q-components is particularly useful at high SNR regime. With the exception of 64-QAM, the P_{cc} of classification with BSS is gradually decreased as Q increases at high SNR regime, while the P_{cc} of classification without BSS becomes gradually lower as Q increases. However, the performance improvement of the classification with BSS is gradually increased compared to the classification without BSS at high SNR regime as Q increases.

V. Conclusion

In this paper, we proposed a hierarchical deep learning method for the waveform and modulation recognition in radar-communications coexistence systems and shared spectrum scenarios. The received signal is first classified as a single carrier radar, communication or multicarrier waveform by using time-frequency FSST representation and deep CNN. In case of multicarrier subclass, OFDM parameters including the CP duration, number of subcarriers and subcarrier spacing are estimated. After isolating the subcarrier signal by the FFT operation, the BSS is employed to make the I- and Q-components of the subcarrier signal as independent as possible. The extracted time-domain signal of each subcarrier is fed into the CNN for the modulation classification.

References

[1] W. S. H. M. W. Ahmad et al., "5G technology: towards dynamic spectrum sharing using cognitive radio networks ," *IEEE Access*, vol. 8, pp. 14460–14488, Jan. 2020.

[2] Z. Slavik and K. V. Mishra, "Cognitive interference mitigation in automotive radars," in *IEEE Radar Conference*, Apr. 2019, pp. 1–6.

[3] S.-H. Kong et al., "Automatic LPI radar waveform recognition using CNN," *IEEE Access*, vol. 6, pp. 4207–4219, Jan. 2018.

[4] J. Lunden and V. Koivunen, "Automatic radar waveform recognition," *IEEE J. Sel. Topics Signal Process.*, vol. 1, no.1, pp. 124–136, Jun. 2007.

[5] M. Zhang, L. Liu, and M. Diao, "LPI radar waveform recognition based on time-frequency distribution," *Sensors*, vol. 16, no.10, pp. 1682–1702, Oct. 2016.

[6] T. J. O'Shea, T. Roy and T. C. Clancy, "Over-the-air deep learning based radio signal classification," *IEEE J. Sel. Topics Signal Process.*, vol. 12, no.1, pp. 168–179, Feb. 2018.

[7] H. Li et al., "OFDM modulation classification and parameters extraction," in *Int. Conf. Cognitive Radio-Oriented Wireless Networks and Communication*, May. 2006, pp. 1–6.

[8] G. Kong and V. Koivunen, "Radar waveform recognition using Fourier-based synchrosqueezing transform and CNN," in *IEEE Int. Workshop Comput. Adv. Multi-Sensor Adaptive Process. (CAMSAP)*, Dec. 2019, pp. 664–668.

[9] G. Kong, M. Jung and V. Koivunen, "Waveform recognition in multipath fading using autoencoder and CNN with Fourier synchrosqueezing transform," in *IEEE Int. Radar Conference*, Apr. 2020, pp. 612–617.

[10] R. Behera, S. Meignen, and T. Oberlin, "Theoretical analysis of the second-order synchrosqueezing transform," *Appl. Comput. Harmon. Anal.*, vol. 45, pp. 379–404, Sep. 2018.

[11] M. Wax and T. Kailath, "Detection of signals by information theoretic criteria," *IEEE Trans. Acoust. Speech Signal Process.*, vol. ASSP-33, pp. 387–392, Apr. 1985.

[12] P. Stoica and T. Soderstrom, "Statistical analysis of MUSIC and subspace rotation estimates of sinusoidal frequencies," *IEEE Trans. Acoust., Speech, Signal Process.*, vol. 39, no.8, pp. 1836–1847, Aug. 1991.

[13] A. Belouchrani, K. A. Meraim, J.-F. Cardoso, and E. Moulines, "A blind source separation technique based on second-order statistics," *IEEE Trans. Signal Process.*, vol. 45, pp. 434–444, Feb. 1997.

[14] J. A. Parker, R. V. Kenyon, and D. Troxel, "Comparison of interpolating methods for image resampling," *IEEE Trans. Med. Imag.*, vol. MI-2, no. 1, pp. 31–39, Mar. 1983.

[15] S. Basiri, E. Ollila and V. Koivunen, "Alternative derivation of fastICA with novel power iteration algorithm," *IEEE Signal Process. Lett.*, vol. 24, no. 9, pp. 1378–1382, Sep. 2017.

[16] A. Hyvarinen, "Fast and robust fixed-point algorithms for independent component analysis," *IEEE Trans. Neural Netw.*, vol. 10, no. 3, pp. 626–634, May 1999.

[17] Ericsson, Rohde and Schwarz, Nokia, and Motorola, "R4-070572: Proposal for LTE channel models," 3GPP TSG RAN WG4, meeting 43, 3GPP, Kobe, Japan, May 2007.

[18] D. P. Kingma and J. Ba, "Adam: A method for stochastic optimization," in *ICLR*, San Diego, CA, May 2015.